Oscillations in Capacitively Coupled Plasmas Induced by Nonlinear Coupling between the Plasma and its External Circuit

Dehen Cao[1], Shimin Yu[2], Jingwen Xu[3], Wei Jiang[1,2], Julian Schulze[4], Ya Zhang[3]

[1] School of Physics, Huazhong University of Science and Technology, Wuhan 430074, China

[2] International Joint Research Laboratory of Magnetic Confinement Fusion and Plasma Physics, State Key Laboratory of Advanced Electromagnetic Engineering and Technology, School of Electrical and Electronic Engineering, Huazhong University of Science and Technology, Wuhan 430074, China

[3] Department of Physics, Wuhan University of Technology, Wuhan 430070, China

[4] Chair of Applied Electrodynamics and Plasma Technology, Faculty of Electrical Engineering and Information Sciences, Ruhr University Bochum, 44801 Bochum, Germany

[5] Corresponding Authors: weijiang@hust.edu.cn and yazhang@whut.edu.cn

19 July 2026

Abstract.

In experiments, periodic oscillations in capacitively coupled plasmas (CCP) driven by a radio frequency (RF) generator can arise from various factors, one of which is the impedance mismatch due to specific system conditions. In this paper, through numerical simulations incorporating an external circuit, we demonstrate that even a highly simplified CCP circuit without any special configurations can generate oscillations caused by such mismatches, and we provide a more in-depth physical explanation of the oscillatory behavior. Our findings reveal that certain circuit component values can lead to significant oscillations in parameters such as electron density and electron temperature, with the oscillation frequency being adjustable by modifying external circuit components. The results also suggest that these oscillations stem from the nonlinear interaction between the plasma and its external circuits. Based on this, we divide the control parameters of the oscillations into two categories: (i) parameters that are part of the external circuit, e.g., the power supply frequency and the values of components in the impedance matching network (IMN). (ii) Parameters that are part of the CCP and affect its resistance and capacitance, such as the electrode spacing and electrode area of the CCP. Additionally, as the oscillations significantly undermine the system's matching performance, we also propose methods to eliminate them.

Keywords: capacitively coupled plasmas, impedance matching, oscillation

(Some figures may appear in colour only in the online journal)

Submitted to: *Plasma Sources Sci. Technol.*

1. Introduction

For applications, capacitively coupled plasmas (CCP) are typically operated in combination with external circuits [1, 2]. These include components such as capacitors, inductors, and impedance matching networks (IMN) [3], as shown in Fig. 1. By adjusting the external circuitry, operators can maximize power absorption in the plasma [4, 5], control the spatial distribution of the plasma [6], and tailor the plasma properties to the specific needs of a process [7, 8]. In many industrial applications such as thin film deposition [9], etching [10, 11], and surface modification [12], an external circuit is indispensable.

However, the interaction between the plasma and the external circuit is non-linear and complex [2, 13], necessitating the use of sophisticated models and simulations for optimization. In our previous work [14], we employed machine learning techniques to optimize impedance matching in the aforementioned CCP system. During this process, we encountered an unexpected phenomenon: When the external circuit or CCP components reached certain specific values, virtually all plasma parameters (current in the CCP branch, voltage drop across the plasma, power absorbed in the plasma, electron density and electron temperature, etc.) exhibited pronounced periodic oscillations that evolved over time. Furthermore, virtually all components in the circuit (the voltage and frequency of the power supply, the specifications of the matching network components, the electrode area and gap distance of the CCP, etc.) can influence the period of these oscillations, but the extent of their impact varies.

There has been considerable research on plasma instabilities and oscillation phenomena in experiments and simulations years ago [15–22]. Katsch et al. [16] observed kHz oscillations in a 13.56 MHz CCP oxygen discharge experimentally, attributing them to an attachment-induced ionization instability due to the presence of negative ions and the dependence of the electron attachment on the electron temperature. Kim et al. [23] observed relaxation oscillations in argon capacitive discharges connected to a peripheral grounded chamber using time-resolved optical emission measurements. They attributed these oscillations to the increased resistance and capacitance of the discharge when the plasma ignites, leading to a loss of overall equilibrium and a subsequent dramatic voltage drop. Küllig et al. [24] experimentally studied instabilities in a capacitively coupled oxygen plasma, relating them to attachment-induced ionization instabilities dependent on the electron temperature and the metastable molecular oxygen density. Most recently, Dong et al. [25] used a hybrid fluid / Monte Carlo approach to connect periodic instabilities in CF_4/Ar radio frequency (RF) CCPs to oscillations in electron density and temperature influenced by electronegativity and drift electric fields. In asymmetric CCPs, self-excited plasma series resonance (PSR) oscillations were observed [20–22]. This phenomenon is triggered by an RLC resonant circuit within the plasma system, where the resistance (R) is caused by electron-neutral collisions, the inductance (L) arises from the electron inertia, and the capacitance (C) originates from the nonlinear capacitance of the RF sheath near the powered electrode. When the driving RF satisfies the resonance condition $\omega^2 = \frac{1}{LC}$, the inductive and capacitive reactance cancel each other out, minimizing the system impedance and significantly amplifying the current. At resonance, energy cyclically transfers between inductive magnetic and capacitive electric forms, leading to sustained oscillations. PSR oscillations typically manifest as high-frequency oscillations above the driving RF and have been found to significantly enhance electron power absorption.

Previous research on CCP oscillations mainly attributed these oscillations to the intrinsic properties of the CCP, such as the influence of electronegative gases. However, as we are about to demonstrate, such oscillations can also be caused by the interaction of the plasma with the external circuit, such as the one observed experimentally by Kim et al. [23]. Their study attributed the observed oscillations to an imbalance in the circuit state caused by a "slot ignite" in the CCP device. However, our results indicate that even the simplest CCP device (with only a central discharge area) can still experience oscillations because of its non-linear interactions with the external circuit. Building on the work of Kim et al., we not only provide a more detailed analysis of the physical origin of such oscillations but also offer suggestions on how to eliminate them.

This paper is organized as follows: In Sec.2, we introduce a numerical simulation method to model a CCP coupled with an external circuit. In Sec.3, we present the observed oscillations and their characteristics, along with the effects of changing each circuit parameter on the oscillations. We first analyze the physical origin of the oscillations, then classify the parameters affecting them, and explain in detail why different parameters have different effects on these oscillations. Finally, in Sec. 4, we provide the conclusions of our study.

2. Method

Fig. 1 presents the circuit model we selected for our simulations. To emphasize the basic mechanisms behind the generation of the oscillations, the circuit comprises only essential components: a radio frequency (RF) generator, an impedance matching network (IMN), and a plasma load.

The power supply maintains a constant source voltage amplitude U_s, a stable driving frequency f_s, and is accompanied by an internal resistance R_s. Although many previous studies and industrial applications used constant power sources - where we also observed similar oscillations in simulations - this study uses a constant voltage source. The reason for this is the fact that, in numerical simulations, the voltage can be set directly to a fixed value, meaning the power regulation is essentially "instantaneous." In contrast, a constant power supply with feedback control interacts with the discharge, leading to a "lag" in power regulation. This delay can cause minor fluctuations in power around the set value, introducing unnecessary instability that may interfere with our analysis of the underlying causes of the observed oscillations. To eliminate these potential instability factors, we use a simple Thévenin model (perfect voltage source in series with a resistor) [3] to represent the power supply.

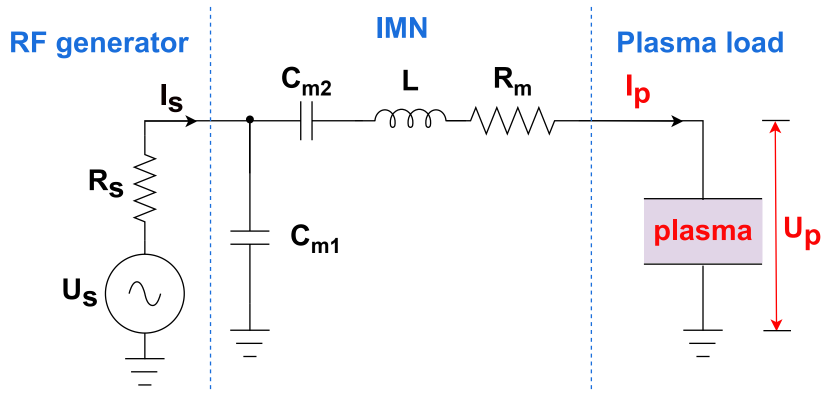

Figure 1. The simulated network, that consists of the plasma coupled with its external circuit. It consists of the radio frequency generator, the impedance matching network, and the plasma load.

The impedance matching network is a typical L-type IMN, which includes two variable capacitors, C_{m1} and C_{m2}, and a variable inductor, L. The resistor, R_m, is used to simulate the power loss of the matching network, following the approach proposed by Schmidt et al. [2].

The single frequency plasma load is modeled by a 1D implicit particle in cell / Monte Carlo collision (PIC/MCC) [26–30] algorithm. The working gas is argon, with a gas temperature of 300 K and a gas pressure of P_p. The identical surface areas of the powered and grounded electrode inside the CCP is A_p, respectively, and the distance between the electrodes is D_p. To reduce simulation time, the initial electron density is set to $1 \times 10^{15}\,\mathrm{m}^{-3}$, indicating that breakdown has already occurred, while in a real discharge process, the electron density would typically start from zero. According to the work of Vass et al. [31], different time steps and spatial steps will significantly influence the simulated electron density. Variations in density alter the sheath thickness, which in turn affects the impedance of the CCP. However, this effect is purely quantitative and does not affect the qualitative conclusions of our oscillation mechanism analysis. To maintain consistency, we fixed the spatial grid size at 3.125×10^{-4} m and the time step at 1.0×10^{-10} s. Moreover, unlike most CCP devices, our plasma load does not include a stray capacitance. This is because oscillations were observed in simulations both with and without stray capacitance, indicating that its presence is not the essential cause of oscillations. To simplify the analysis and focus on the core mechanism, we excluded the stray capacitance.

At low pressures ($\sim$ 10 Pa), metastable particles are considered to have a minimal impact on ionization in the plasma bulk. Previous studies have shown that direct ground-state ionization is the dominant process at these pressures [32–34]. Tracking metastable particles in PIC/MCC simulations is computationally expensive. As a result, most current particle-based modeling studies omit excited-state atoms with relatively low density [35, 36]. We follow this approach and do not include metastable particles in our model. Our MCC model incorporates the elastic, excitation, and ionization collisions of electrons with neutral particles as well as the elastic scattering and charge-exchange collisions of ions with neutral particles. We assume that the neutral particles are stationary and uniformly distributed, since the total degree of ionization is less than 0.01%. These collisions are simulated using random numbers and collision cross sections, with the electron and ion collision models based on the work of Yamabe et al. [37] and Phelps et al. [38], respectively, and the specific interaction cross-section data sourced from the LXCat Phelps database [39]. For further details on the code implementation, refer to the repository [40].

The impedance of the CCP is determined based on the voltage drop across the CCP and the current flowing through the plasma, according to Eq.1:

$$\begin{aligned} Z_{CCP} &= \frac{U_p}{I_p}\cos\varphi + j\frac{U_p}{I_p}\sin\varphi \\ &= R + jX, \end{aligned} \tag{1}$$

where U_p is the amplitude of the voltage waveform that drops across the plasma, I_p is the amplitude of the current waveform, φ is the phase difference between the voltage and current waveforms, R is the real part of the impedance which represents the resistance, j is the imaginary unit, and X is the imaginary part of the impedance which represents the reactance. All these parameters are considered at the driving frequency f_s. The equation thus separates the impedance into its resistive (R) and reactive (X) components, providing information on the energy dissipation and storage properties of the CCP system, respectively.

The plasma is coupled self-consistently to the external circuit based on iteratively solving Kirchhoff's law for the network shown in Fig. 1 and the PIC / MCC simulation of the plasma for a set of fixed elements of the external circuit. This procedure is described in detail in our previous work [41, 42]. Moreover, it is important to note that due to simplifications in modeling the power supply and stray capacitance of the plasma load, the numerical circuit parameters and quantitative results may differ significantly from those of a real CCP device. Nevertheless, as we will demonstrate later, this simplified model is not only sufficient to generate oscillations but also makes the analysis of these oscillations particularly clear.

3. Results

Firstly, the oscillatory phenomenon along with a description of its main characteristics is presented in section 3.1. Then a detailed analysis of its physical origin is performed in section 3.2, leading to a classification of circuit parameters that affect the oscillations, into external circuit parameters and internal plasma parameters. Sections 3.3 and 3.4 finally discuss the effects of these control parameters on the oscillation phenomenon separately.

3.1. Basics of the plasma oscillation phenomenon

Table 1. Examples of simulation input parameters that result in stable and oscillatory discharge conditions.

mode	$U_{s(\mathrm{V})}$	$f_{s(\mathrm{MHz})}$	$R_{s(\Omega)}$	$C_{m1(\mathrm{pF})}$	$C_{m2(\mathrm{pF})}$	$L_{(\mu\mathrm{H})}$	$R_{m(\Omega)}$	$D_{p(\mathrm{m})}$	$A_{p(\mathrm{m}^2)}$	$P_{p(\mathrm{Pa})}$
STABLE	350	13.56	50.0	329.6	230.2	6.32	0.5	0.03	$\pi\times0.1^2$	13.3
OSCI	350	14.0	50.0	329.6	230.2	6.32	0.5	0.03	$\pi\times0.1^2$	13.3

Table 1 contains two exemplary sets of input parameters of the simulations (see Fig. 1) that differ from each other only in terms of a slight change of the driving frequency from 13.56 MHz to 14.0 MHz. The elements of the IMN are selected so that good matching is realized at 13.56 MHz. Then these parameters are kept the same at 14.0 MHz. Our simulations show that this small difference in driving frequency results in completely different discharge characteristics, i.e., it induces a transition from a stable (13.56 MHz) to an oscillatory (14.0 MHz) operation mode. While in the stable mode all plasma parameters are stable, they fluctuate considerably as a function of time in the oscillatory mode.

Fig. 2 shows selected results obtained from the simulation in both modes (stable left column, oscillatory right column) in terms of the electron density (first row), amplitude of the voltage waveforms at the RF generator and of the voltage drop across the plasma (second row), current in the generator and in the plasma (third row), power output of the generator, power absorbed by the CCP, power reflected back to the generator (fourth row) and the electron temperature (fifth row). The electron density and temperature are shown with spatial resolution between the electrodes. The time axis covers several thousands of consecutive RF periods, i.e., dynamics on relatively long timescales are discussed, well beyond the dynamics within an RF period. In the stable mode at 13.56 MHz, the simulation converges in a classical way so that all parameters are stable as a function of time on timescales beyond a single RF period. Meanwhile, the near-zero steady-state reflected power indicates effective impedance matching. However, as shown in the right column of Fig. 2, the discharge characteristics of the CCP will be distinctly different, if the discharge is driven at 14.0 MHz. Now, all plasma parameters exhibit periodic oscillations at a frequency of approximately 10 kHz. The spatiotemporally resolved results for the electron density and the time resolved power absorption by the plasma indicate that the plasma undergoes a continuous cycle of extinguishing and reignition, i.e., the plasma between the electrodes builds up to a certain level and then rapidly disappears, followed by a reignition.

3.2. Physical origin of plasma oscillations

To reveal the physical origin of the observed plasma oscillations, we analyze the impedance matching between the RF generator and the total load shown in Fig. 1. The total impedance of the IMN and the plasma is:

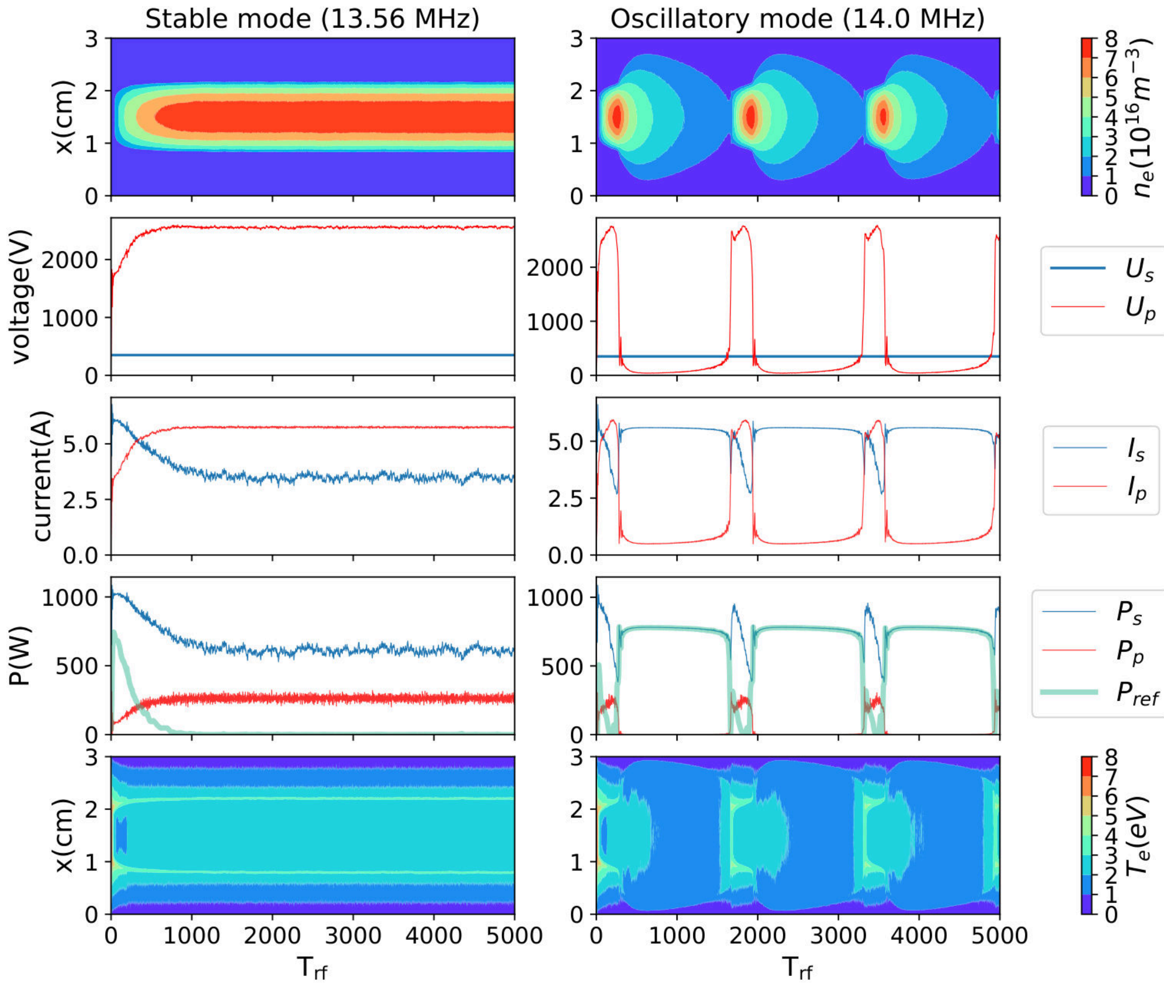

Figure 2. The spatiotemporal evolution of the CCP's parameters corresponding to the two modes. Left column: stable; right column: oscillatory. 1st row: Electron density. 2nd row: Power supply voltage (blue line), voltage across the CCP (red line). 3rd row: Current in the power supply branch (blue line), current in the CCP branch (red line). 4th row: Power output of the power supply (blue line), power absorbed by the CCP (red line), power reflected back to the power supply (light green line, calculated as $P_{ref} = |\Gamma|^2 * P_s$, where $|\Gamma|$ is the reflection coefficient defined in Eq. 6). 5th row: Electron temperature. The horizontal axis represents the RF cycle.

$$Z_{load} = \frac{Z_1 * Z_2}{Z_1 + Z_2}, \tag{2}$$

where

$$\begin{aligned} Z_1 &= Z_{C_{m2}} + Z_L + Z_{R_m} + Z_p \\ &= -j\frac{1}{\omega C_{m2}} + j\omega L + R_m + R_p - j\frac{1}{\omega C_p} \\ &= (R_m + R_p) + j(\omega L - \frac{1}{\omega C_{m2}} - \frac{1}{\omega C_p}) \end{aligned} \tag{3}$$

and

$$\begin{aligned} Z_2 &= Z_{C_{m1}} \\ &= -j\frac{1}{\omega C_{m1}}. \end{aligned} \tag{4}$$

Here, Z_p represents the equivalent impedance of the plasma, while R_p and C_p correspond to the equivalent plasma resistance and capacitance derived from this impedance, respectively. $\omega = 2\pi f_s$, where f_s is the driving RF.

Since the power source contains only an internal resistance, its impedance is:

$$Z_s = R_s. \tag{5}$$

Then for the circuit shown in Fig. 1, we can calculate the magnitude of the reflection coefficient:

$$\begin{aligned} |\Gamma| &= |\frac{Z_{load} - Z_s}{Z_{load} + Z_s}| \\ &= |\frac{Re(Z_{load}) - R_s + j * Im(Z_{load})}{Re(Z_{load}) + R_s + j * Im(Z_{load})}| , \end{aligned} \tag{6}$$

where $|\Gamma|$ closer to 0 indicates better impedance matching. For convenience, we refer to it as the "reflection coefficient" in the following sections.

After setting the parameters shown in Table 1, all circuit parameters in the circuit shown in Fig. 1 are fixed, except the equivalent capacitance and equivalent resistance of the plasma. Therefore, we can rewrite Eq. 6 as:

$$|\Gamma| = f(C_p, R_p). \tag{7}$$

And when the parameters are set to those resulting in the oscillatory mode, the distribution of $|\Gamma|$ for this equation within the parameter space $\{C_p \in (15\text{ pF},\ 40\text{ pF})\} \cap \{R_p \in (0\,\Omega,\ 30\,\Omega)\}$ is shown in Fig. 3. The white line represents the real-time trajectory of the plasma over a single oscillation period (the second period of the oscillatory mode in Fig.2). As marked by I (yellow line segment) and II (grey line segment), the plasma undergoes two abrupt changes in the reflection coefficient within this period. Specifically, at I, the reflection coefficient rapidly increases from 0 to 1, while at II, it sharply drops from 1 to 0. It should be noted that although the regions at the start and end points are also transition regions, we will later explain why only the areas marked I and II lead to oscillations.

To reveal what happens at these transition regions, Fig. 4 illustrates the temporal variations of various plasma parameters during the oscillation period. Initially, from 1600 T_{rf} to the region marked by the yellow background (Area I), as gas ionization advances, plasma rapidly accumulates. This accumulation refers to the gradual increase in charged particles, primarily electrons and ions, within the discharge region due to ionization driven by the applied electric field. The resulting increase in electron density significantly enhances the plasma's electrical conductivity, leading to a swift rise in plasma current. However, sustaining additional plasma requires more energy. Thus, the voltage across the CCP electrodes and absorbed power increase correspondingly.

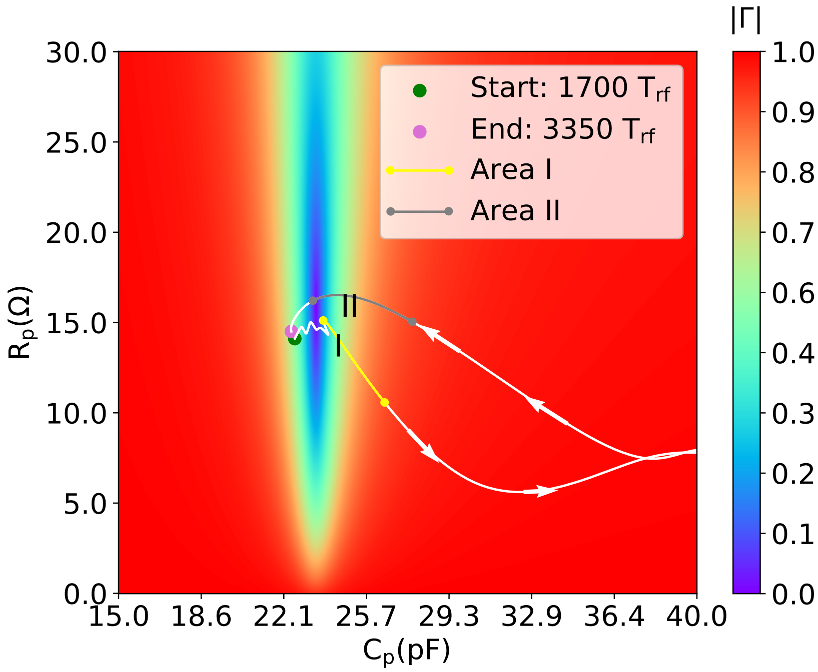

Figure 3. Reflection coefficient as a function of the plasma capacitance, C_p, and resistance, R_p, for the oscillatory scenario (see Fig. 2). The white line shows the real-time variation of the reflection coefficient during one oscillation period, from the 1700th to the 3350th RF cycle. I and II indicate regions of strong changes in the reflection coefficient.

Concurrently, the elevated electron density compresses the sheath, reducing its thickness. According to

$$C_s = \frac{\varepsilon_0 A}{s}, \tag{8}$$

(where ϵ_0 is the vacuum permittivity), the decreased sheath thickness s leads to an increased sheath capacitance C_s, which raises the plasma's equivalent capacitance. The capacitance increases is so small that it is not easily distinguishable in Fig. 4. However, in Fig. 3, this increase is clearly reflected in the rightward shift of its trajectory toward a better matching region (from the green starting point to the initial position of area I). This shift enhances the power absorption efficiency of the CCP, triggering a positive feedback loop with a continuous increase in electron density, voltage drop, and plasma current. However, an increase of C_p causes a further rightward shift of the trajectory and will lead it into region I, where even a slight increase in capacitance will rapidly drive the reflection coefficient close to 1. As shown in Fig. 4, when passing through region I, the rapid rise in the reflection coefficient results in a slight decrease in both the voltage across the plasma and the current, leading to reduced power absorption by the CCP. This mechanism is self-amplifying in the sense that now, due to these initially small changes of the plasma parameters, the plasma capacitance and resistance change in a way that reduces the matching quality even more. Due to this change of the plasma impedance

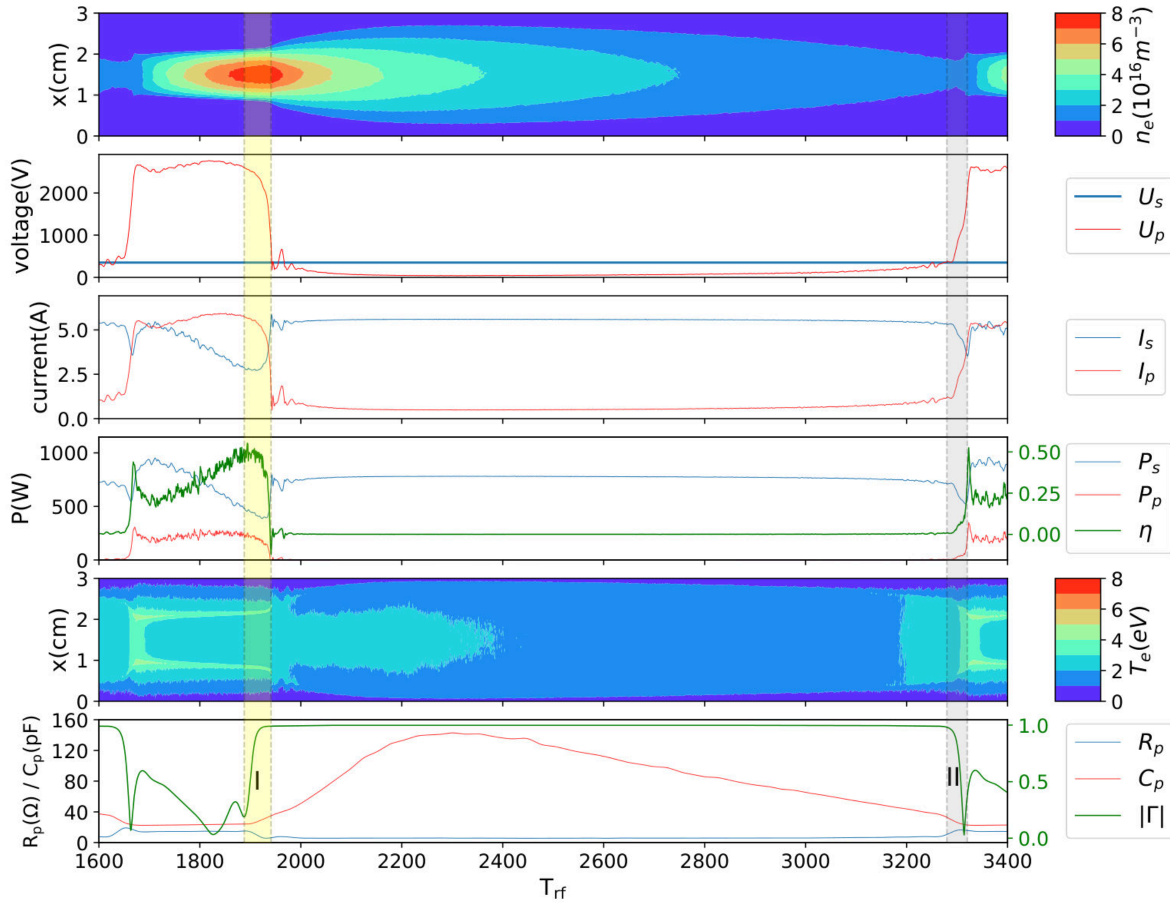

Figure 4. Evolution of plasma parameters within a single oscillation period: Electron density (first row), voltage at the RF generator and across the CCP (second row), current in the power supply branch and in the plasma (third row), power output of the generator, power absorbed by the plasma and power absorption efficiency (defined as $\eta = P_p/P_s$) of the CCP (fourth row), electron temperature (fifth row), and equivalent resistance, capacitance, and reflection coefficient ($|\Gamma|$) of the CCP (sixth row). The horizontal axis represents the RF cycle.

at fixed impedance of the IMN, the total load impedance changes. Consequently, the current in the source increases. These abrupt changes initiate high frequency oscillations of the plasma and source current as well as the power dissipation in the discharge and the plasma resistance, which are damped after about 100 RF periods. Meanwhile, the reduction in input power results in a continuous decline in both electron density and temperature. After crossing region I and the high-frequency oscillations have stabilized, the voltage across the CCP electrode plates approaches zero, significantly reducing the electric field between the electrodes. This prevents electrons from acquiring sufficient energy, markedly decreasing the ionization rate and severely inhibiting new plasma generation within the plates. In the absence of a strong electric field, electrons diffuse along concentration gradients towards areas of lower density, such as the electrodes and chamber walls. The combined effects of reduced sheath voltage and electron diffusion decrease the sheath thickness. According to Eq.8, this increases the plasma's equivalent capacitance, shifting the trajectory further rightward (Fig. 3). However, as the electron density further decreases, it reaches a critical threshold (around the 2300th RF cycle in Fig.4) where the density gradient is insufficient to maintain diffusion. At this point, the Debye length, calculated using the formula

$$\lambda_D = \sqrt{\frac{\varepsilon_0 k_B T_e}{n_e e^2}}, \tag{9}$$

(where k_B is Boltzmann's constant, T_e is the electron temperature, n_e is the electron density, e is the elementary charge), increases significantly. This is primarily due to a more pronounced reduction in electron density (n_e) relative to the electron temperature (T_e). The resulting increase in Debye length leads to a thicker sheath, reducing the plasma's capacitance and shifting its trajectory leftward (Fig. 3). When the trajectory shifts leftward into transition region II, the reflection coefficient swiftly approaches zero, reinitiating a rapid plasma accumulation phase via the positive feedback loop. As before, the rise in electron density will again compress the sheath, thinning it and increasing the plasma's capacitance. As illustrated in Fig. 3, the trajectory will shift right once more, and trigger a new oscillation period upon returning to region I.

Overall, the most direct cause of oscillatory behavior is density collapse during the accumulation process of plasma. This collapse results from dynamic interactions among plasma diffusion, sheath behavior, and changes in plasma parameters triggered by a surge in the reflection coefficient. The CCP system is initially in a well-matched region. As the reflection coefficient swiftly increases from near zero to one, the CCP system rapidly transitions from a well-matched state to a mismatched state through a self-amplifying mechanism. Subsequently, in the absence of a strong electric field, ambipolar diffusion driven by density gradients becomes dominant, leading to plasma diffusion towards the electrodes. This results in reduced plasma density and sheath thickness, and an increased capacitance of the plasma. As the plasma density further decreases, insufficient to sustain the diffusion process, sheath expansion dominated by the increase in Debye length becomes predominant. Consequently, the plasma's capacitance decreases, returning it to the initial well-matched region and completing a full oscillation period.

It is worth noting that the oscillatory behavior observed here shares certain characteristics with what is commonly referred to as a "breathing mode" [43–46] in plasma physics. Breathing mode typically involves periodic expansions and contractions of plasma parameters, such as the electron density and temperature, analogous to the way a biological organism breathes. In such a mode, the plasma undergoes self-consistent oscillations, where energy dynamics within the plasma itself drive the periodic behavior. In our case, the oscillatory mode exhibits similar periodic behavior. The electron density, electron temperature, sheath thickness, and power absorbed by the plasma all oscillate over time. Specifically, as the electron density increases, the sheath compresses, and as the plasma density decreases, the sheath expands, akin to the cyclic expansion and contraction characteristic of a breathing mode. However, the key distinction between the oscillatory mode observed here and the classical breathing mode lies in the driving mechanism. The traditional breathing mode is typically intrinsic to plasma dynamics, driven by a cyclic instability where increasing ionization rates deplete neutral particles, causing plasma collapse and subsequent regeneration as neutrals refill the region. In contrast, the oscillations in our study are externally driven by interactions between the CCP and its external circuit, primarily due to impedance mismatches. Here, plasma collapse results from poor matching conditions, not from neutral particle depletion as in the breathing mode. The external circuit plays a critical role in determining the oscillation period, amplitude, and the conditions under which these oscillations occur. Therefore, while our observed oscillatory mode exhibits qualitative similarities with a breathing mode, the physical origin of the oscillations in our system is fundamentally different. Instead, similar to the analysis by Kim et al. [23], the oscillatory behavior observed here closely resembles relaxation oscillations, a well-known phenomenon in nonlinear dynamical systems [47–49]. Relaxation oscillations are characterized by a slow buildup of stress followed by a rapid release, then repeating the cycle periodically. In our system, the external circuit gradually increases "stress" on the plasma load (supplying RF power to a unmatched plasma discharge) until it becomes too strong (impedance mismatch caused by a large drift in the nonlinear discharge capacitance), leading to sudden release (plasma extinction). After extinction, impedance matching improves, the applied voltage rises, reigniting the discharge and restarting the cycle. This slow-fast-slow dynamic aligns closely with relaxation oscillations. Additionally, the oscillation frequency of approximately 10 kHz, significantly lower than the RF driving frequency of 13.56 MHz, further supports this classification, as relaxation oscillations typically occur on timescales longer than the driving period.

For the case of a stable discharge driven at 13.56 MHz and otherwise identical conditions (see Table 1), the real-time evolution of the reflection coefficient, $|\Gamma|$, as a function of the plasma capacitance and resistance is shown in Fig. 5. The reduction in driving frequency shifted the transition region from approximately 24 pF to 26 pF. By the time the plasma reaches about 25.5 pF, it has already accumulated sufficient density to achieve the energy balance for a self-sustained discharge, reaching steady state earlier. Consequently, as this process did not involve a sudden increase in the reflection coefficient from 0 to 1, it did not trigger a density collapse, resulting in a stable discharge mode.

Furthermore, a comparison of Fig. 3 and Fig. 5 reveals three key positions during the oscillation process: (i) initial location of the plasma, (ii) termination location, and (iii) the location of the transition region. As the plasma accumulates, the sheath is compressed due to the rising electron density, resulting in an increase in its equivalent capacitance. This means that plasma accumulation always causes its trajectory to shift to the right. Therefore, if the initial position is to the right of the transition region or the termination position is to the left of it (see Fig. 5), no oscillation will occur. An oscillation is triggered when the transition region lies along the plasma's

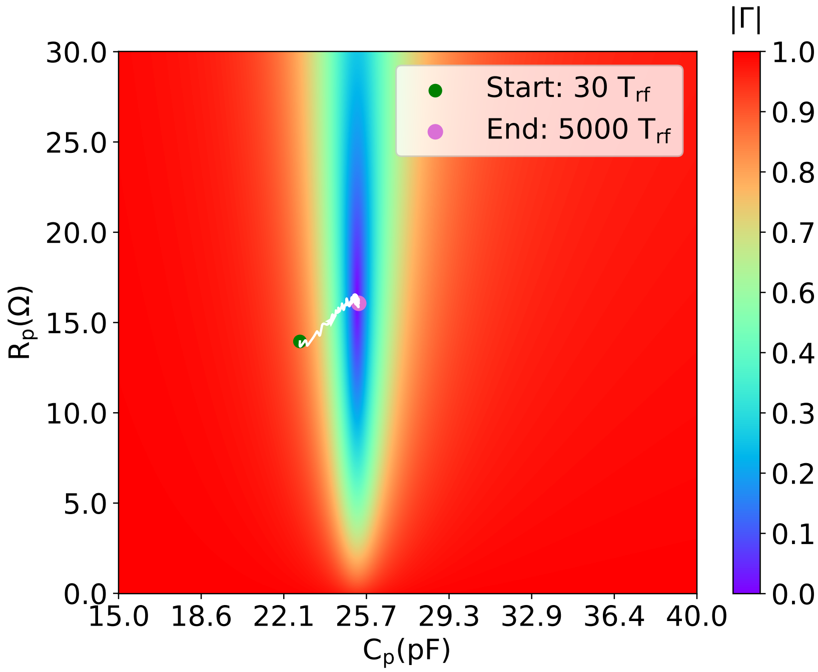

Figure 5. Reflection coefficient as a function of the plasma capacitance, C_p, and resistance, R_p for the stable scenario (see Fig. 2). The white line indicates the change of the reflection coefficient as a function of time.

evolutionary path. According to Eq. 7, the position of the transition region can be explicitly determined by external circuit parameters, while the initial and termination positions of the plasma are primarily influenced by factors that affect its impedance, such as the geometric parameters of the CCP. Therefore, we categorize the components in Fig. 1 into two categories, (i) external circuit parameters and (ii) internal plasma parameters, i.e., adjustable characteristics of the plasma reactor that will affect the plasma impedance such as the electrode gap and surface area. In the following two subsections we will discuss the effects of adjusting these two types of parameters on the plasma oscillations separately.

3.3. Effects of external circuit parameters on plasma oscillations

The characteristics of the external circuit are adjustable by changing the capacitances, inductance, and resistance of the IMN as well as the resistance of the RF generator and the driving frequency according to Fig. 1. The reflection coefficient obtained based on Eq. 6 directly depends on these external circuit parameters. Here, we exemplarily vary the driving frequency, f_s, and the serial capacitance of the IMN, C_{m2}, to study how changing these components affect the oscillatory behavior of the plasma. When adjusting either f_s or C_{m2}, all other components in the circuit remain fixed.

Fig. 6 illustrates the trajectory variations of the plasma in the parameter space (C_p, R_p) (left column) and the corresponding spatio-temporal evolution of the electron

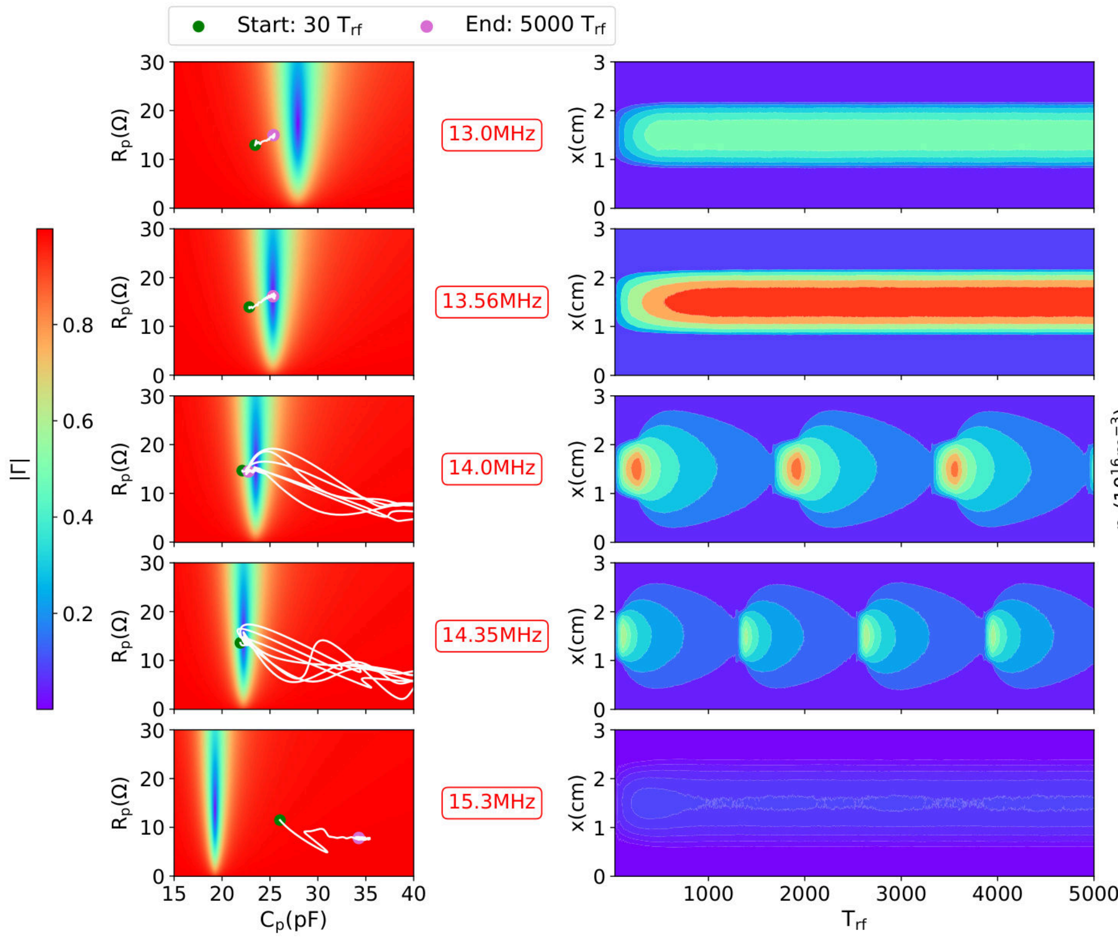

Figure 6. The evolution of plasma at different driving frequencies. Left column: The reflection coefficient as a function of plasma capacitance (C_p) and resistance (R_p), with the white line showing the real-time evolution of the reflection coefficient over time. Right column: Spatiotemporal evolution of plasma electron density. Note: The start and end points of the white line on the left correspond to the initial and final cycles on the right.

density (right column) when only the driving frequency is altered while maintaining all other control parameters constant. These results show that as the driving frequency increases, the position of the transition region and the ideal matching window ($\Gamma \approx 0$) shift to the left, corresponding to a smaller plasma capacitance. At a driving frequency of 13.0 MHz, the plasma's self-sustaining discharge equilibrium position is to the left of the transition region and at the edge of the ideal matching window, exhibiting a stable discharge mode. When the frequency increases to 13.56 MHz, the plasma's equilibrium position shifts into the ideal matching window because of the window's leftward movement, corresponding to a significantly increased electron density while maintaining a stable discharge. At 14.0 MHz, the transition region intersects the plasma's evolution path, resulting in an oscillatory discharge mode. The 14.35 MHz case demonstrates that the closer the starting position is to the transition region, the higher the oscillation frequency. At 15.3 MHz, both the ideal matching window and transition region have moved left of the plasma's initial position, resulting in a stable discharge mode with very low electron density. Thus, a simple stability criterion can be formulated: The discharge is stable when impedance matching continues to improve as the discharge capacitance stabilizes. Moreover, the above analysis indicates that when oscillations occur, adjusting the driving frequency either upward or downward can eliminate them, and appropriately lowering the driving frequency can achieve optimal matching while suppressing oscillations. However, since the oscillation-triggering region is so close to the matching window, methods like frequency tuning to optimize matching may inadvertently enter the oscillation-triggering region instead of the matching window. If forward and reflected power measurements are time-averaged over periods longer than a few milliseconds, the oscillations may go undetected. Additionally, the oscillation frequency is relatively high (∼10 kHz) and likely invisible to the naked eye. In such cases, experimentalists may misinterpret the situation as poor matching, miss the optimal matching window, and experience longer matching times than initially expected.

The effects of changing the IMN serial capacitor, C_{m2}, on plasma behavior are shown in Figs. 7. Initially, when C_{m2} is small (90 pF), the plasma lies in the mismatched region on the left side of the matching window. As the value of C_{m2} increases, the position of the transition region and the ideal matching window shift to lower values of plasma capacitance, similar to the effect of increasing f_s. However, when the value of C_{m2} further increases, the position of these regions stabilizes. This means that selecting a low value C_{m2} results in the ideal matching window being positioned at high plasma capacitances, thus maintaining the CCP in a stable discharge mode. As C_{m2} increases, the critical region moves to the lower values of the plasma capacitance, transferring the CCP into an oscillating discharge mode. Increasing C_{m2} further will not eliminate these oscillations. The reason for this phenomenon is that in our simulated circuit, C_{m2} and L are connected in series. The reactance of the C_{m2} capacitor is negative, while that of the L coil is positive. The purpose of the adjustable C_{m2} capacitance in series with the fixed L coil is to synthesize an adjustable inductor by partially canceling the inductance of the fixed L coil. The effective inductance is given by:

$$L_{\mathrm{eff}} = \frac{L\omega - \left(\frac{1}{C_{\mathrm{m2}}\omega}\right)}{\omega}. \tag{10}$$

At a driving frequency of 13.56 MHz, the reactance of L (6.32 μH) is approximately $2\pi \times 13.56 \times 10^6 \times 6.32 \times 10^{-6} \approx 538.4\,\Omega$, whereas the reactance of C_{m2} (2500 pF) is $-1/(2\pi \times 13.56 \times 10^6 \times 2500 \times 10^{-12}) \approx -4.7\,\Omega$. Thus, when the series capacitance is very large, its effect is negligible compared to the series inductance, leading to $L_{\mathrm{eff}} \approx L$. Consequently, in Fig. 7, as C_{m2} further increases, its modulation effect on the oscillation diminishes.

Furthermore, as shown in Fig. 7, as C_{m2} increases, the transition region shifts leftward while its width gradually narrows. This change amplifies the system's sensitivity to variations in nonlinear plasma impedance because the reduced width of the

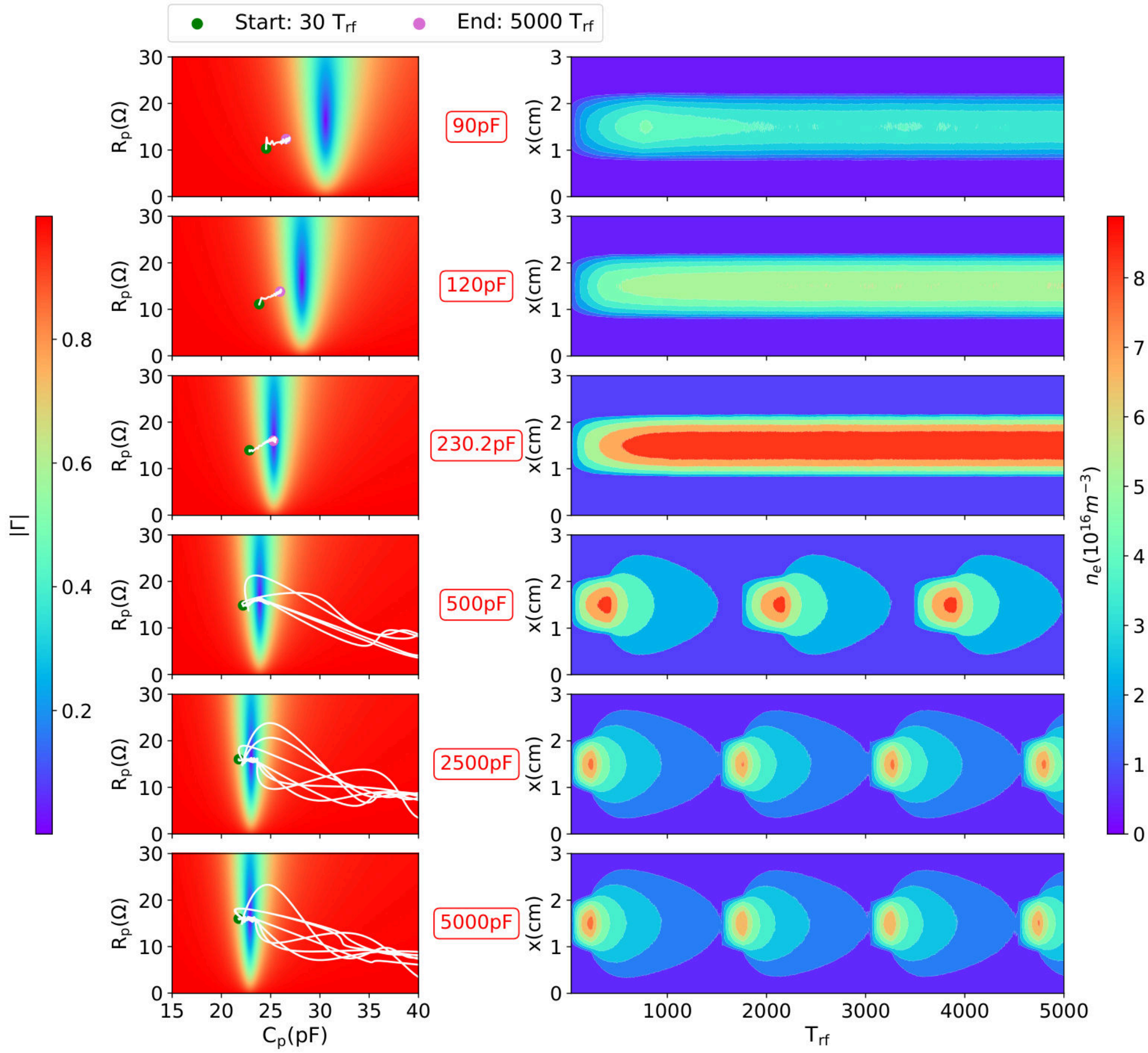

Figure 7. The evolution of plasma for different values of C_{m2}. Left column: The reflection coefficient as a function of plasma capacitance (C_p) and resistance (R_p), with the white line showing the real-time evolution of the reflection coefficient over time. Right column: Spatiotemporal evolution of the plasma electron density. Note: The start and end points of the white line on the left correspond to the initial and final cycles on the right. In practical circuits, capacitors rarely reach such high values, the large capacitance used here serves only to illustrate its effect.

transition region makes it easier for small shifts in plasma impedance to cross it, thereby triggering oscillations. At high C_{m2} values, the external series capacitive reactance becomes negligible, allowing the inherent capacitance of the plasma sheath (C_p) to dominate as the primary negative reactance in impedance matching. This dominance increases the influence of the plasma's equivalent capacitance on the circuit's matching state. Consequently, variations in sheath capacitance, such as those driven by dynamic adjustments in sheath thickness due to changes in electron density, temperature, or electric fields, have a more direct impact on abrupt transitions in the reflection coefficient

$|\Gamma|$ (e.g., regions I and II in Fig. 3). This effect significantly raises the likelihood of oscillation initiation. In practical circuits, the presence of stray capacitance may weaken the dominant role of plasma impedance in the overall matching state of the system. If this weakening effect is significant enough, the resulting shift in plasma capacitance may become too small to cross the transition region, thereby preventing oscillations.

3.4. Effects of internal plasma parameters on plasma oscillations

In this section, we vary the area of the CCP electrodes, A_p, as an example to illustrate the different analytical approaches for external circuit parameters and internal plasma parameters, as well as how the internal plasma parameters influence the behavior of discharge oscillations.

The capacitance of a parallel plate capacitor is:

$$C = \frac{\epsilon_r * \epsilon_0 * A_p}{d}, \tag{11}$$

where ϵ_r is the relative permittivity of the medium, ϵ_0 is the permittivity of vacuum, A_p represents the area of the two plates, and d is the distance between the two plates.

Substitution of Eq.11 into Eq.7 yields the following expression for the reflection coefficient:

$$|\Gamma| = f(R_p, \epsilon_r, A_p). \tag{12}$$

Using the expression above for the reflection coefficient, we attribute changes in the CCP state to changes in its corresponding equivalent resistance, R_p, relative permittivity, ϵ_r (which should more accurately be called equivalent permittivity) and electrode surface area, A_p. The reason for this is that external circuit parameters, such as driving frequency and matching network components, are explicitly embedded in the equations defining the matching window, thus directly determining the transition region's location. These parameters can be analyzed in the plasma impedance space (C_p, R_p), as depicted in Figs. 6 and 7. However, internal parameters not explicitly included in these equations must be transformed to be incorporated into the matching window description. For example, electrode area here can be coupled into the matching window equations using the parallel-plate capacitance formula (Eq. 11), allowing its effect to be equivalently represented as the influence of relative permittivity. Therefore, we perform the analysis in the (ϵ_r, R_p) space, with corresponding results presented in Fig. 8. These results show a similar effect compared to that caused by a variation in the driving frequency, f_s. The increase in A_p also leads to a continuous leftward shift of the transition region and the ideal matching window, causing the CCP to undergo a "stable-oscillatory-stable" mode transition.

4. Conclusions

In this study, we investigate and analyze the oscillations of the CCP in the kilohertz range driven by an RF generator and coupled to an external circuit through numerical

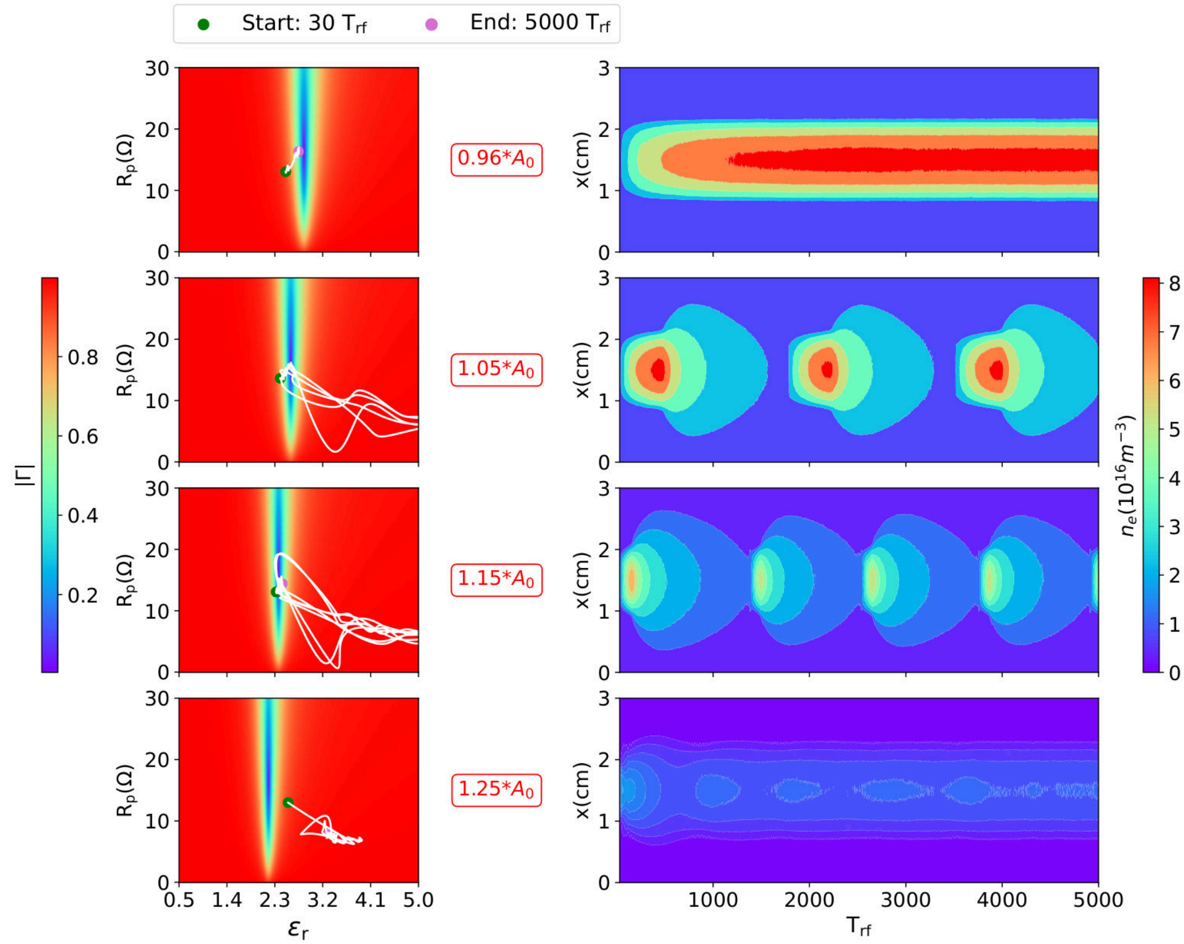

Figure 8. The evolution of plasma for different areas of the CCP electrodes. Left column: The reflection coefficient as a function of plasma equivalent permittivity (ϵ_r) and resistance (R_p), with the white line showing the real-time evolution of the reflection coefficient over time. Right column: Spatiotemporal evolution of the plasma electron density. Note: The start and end points of the white line on the left correspond to the initial and final cycles on the right.

simulations. Our research indicates that two conditions must be met to generate oscillations: (i) the existence of a transition region in the impedance matching and (ii) this region must lie along the plasma evolution path. When both conditions are satisfied, the CCP passes through the transition region before reaching steady state, triggering density collapse and leading to oscillations. In fact, similar oscillations triggered by mismatching were observed in the experiment by Kim et al. [23] long ago. In their study, these oscillations were essentially caused by slot ignition, which induced a sudden change in impedance matching, representing a transition region due to specific system conditions. However, our analysis shows that oscillations can arise even in a highly simplified circuit without any special conditions.

Additionally, based on the analysis in the plasma impedance space, we identify three key locations closely related to the oscillation process: (i) initial location of the plasma, (ii) termination location, and (iii) the location of the transition region. We then classify the parameters governing the oscillation into two types: external circuit parameters and intrinsic CCP parameters. External parameters, such as the driving frequency, directly appear in the reflection coefficient equation and thus determine the transition region's location. In contrast, intrinsic parameters, such as electrode area, affect the plasma impedance, thereby determining the initial and termination positions. When the transition region lies between the initial and termination positions of the plasma, oscillation is triggered, and the closer the initial position is to the transition region, the higher the corresponding oscillation frequency.

However, because of the narrow transition region and high sensitivity to specific parameters, this oscillatory behavior may only occasionally occur during the actual optimization process. Additionally, several factors may contribute: (i) Certain circuit component values may eliminate the so-called matching transition region, preventing any state transitions and thereby avoiding plasma collapse. (ii) Stray capacitance may reduce the relative discharge capacitance offset seen from the output of the matching network, diminishing the plasma impedance's dominance over circuit matching. If this offset is sufficiently small, the plasma remains entirely within the smooth portion of the transition region without crossing it, preventing oscillations from being triggered. (iii) Losses in the actual circuit may affect the width of the transition region, similarly keeping the plasma within the smooth portion of the transition zone. For circuits capable of producing a transition region, the ideal matching window is also obviously quite narrow. In this situation, the better the match, the more likely oscillations will be triggered. But this also means that if one encounters CCP oscillations during the experiment, a well-matched region is not far away. This essentially implies a new matching strategy, where optimal matching can be achieved either by adjusting the steady-state position of the plasma within the (C_p, R_p) space to the ideal matching window or by adapting the window to the plasma's steady-state position.

It should be noted that, in this paper, we employ a highly simplified circuit model to analyze the physical origins of oscillations caused by mismatch. To focus on the core mechanism, many model details have been omitted. Building on this foundation, future work will involve developing more advanced and realistic circuit models to facilitate experimental validation. Additionally, further quantitative analyses, such as exploring the dependence of oscillation frequency on external circuit parameters, will be discussed in subsequent research.

Acknowledgments

This work was supported by the National Natural Science Foundation of China (12275095, 11975174 and 12011530142) and the German Research Foundation in the frame of project 428942393.

OICIDs

Dehen Cao https://orcid.org/0009-0006-8038-9176
Shimin Yu https://orcid.org/0000-0002-3832-5252
Jingwen Xu https://orcid.org/0000-0003-1385-3320
Wei Jiang https://orcid.org/0000-0002-9394-585X
Julian Schulze https://orcid.org/0000-0001-7929-5734
Ya Zhang https://orcid.org/0000-0003-0473-467X

Data Availability Statement

The data that support the findings of this study are available from the corresponding author upon reasonable request.

Conflict of interest

The authors have no conflicts of interest to disclose.

References

[1] Bera K, Rauf S, Balakrishna A and Collins K 2010 *IEEE Transactions on Plasma Science* **38** 3241–3248 ISSN 0093-3813 URL http://ieeexplore.ieee.org/document/5625075/

[2] Schmidt F, Mussenbrock T and Trieschmann J 2018 *Plasma Sources Science and Technology* **27** 105017 ISSN 1361-6595 URL https://iopscience.iop.org/article/10.1088/1361-6595/aae429

[3] Lieberman M A and Lichtenberg A J 2005 *Principles of Plasma Discharges and Materials Processing* 1st ed (Wiley) ISBN 978-0-471-72001-0 978-0-471-72425-4 URL https://onlinelibrary.wiley.com/doi/book/10.1002/0471724254

[4] Qu C, Lanham S J, Shannon S C, Nam S K and Kushner M J 2020 *Journal of Applied Physics* **127** 133302 ISSN 0021-8979, 1089-7550 URL https://pubs.aip.org/jap/article/127/13/133302/156794/Power-matching-to-pulsed-inductively-coupled

[5] Poulose J, Goeckner M, Shannon S, Coumou D and Overzet L 2017 *The European Physical Journal D* **71** 242 ISSN 1434-6060, 1434-6079 URL http://link.springer.com/10.1140/epjd/e2017-80096-7

[6] Bera K, Rauf S, Ramaswamy K and Collins K **106** 033301 ISSN 0021-8979, 1089-7550 URL https://pubs.aip.org/aip/jap/article/370509

[7] Yamazawa Y 2015 *Plasma Sources Science and Technology* **24** 034015 URL https://dx.doi.org/10.1088/0963-0252/24/3/034015

[8] Lim Y M, He Y, Lee J, Kim J H, Kim K H and Chung C W 2022 *Plasma Sources Science and Technology* **31** 065006 URL https://dx.doi.org/10.1088/1361-6595/ac56c4

[9] Michelmore A, Whittle J D, Short R D, Boswell R W and Charles C 2014 *Plasma Processes and Polymers* **11** 833–841 ISSN 1612-8850, 1612-8869 URL https://onlinelibrary.wiley.com/doi/10.1002/ppap.201400026

[10] Makabe T and Petrović Z 2002 *Applied Surface Science* **192** 88–114 ISSN 01694332 URL https://linkinghub.elsevier.com/retrieve/pii/S0169433202000223

[11] Wang M and Kushner M J 2010 *Journal of Applied Physics* **107** 023309 ISSN 0021-8979, 1089-7550 URL https://pubs.aip.org/jap/article/107/2/023309/399014/High-energy-electron-fluxes-in-dc-augmented

[12] Upadhyay J, Im D, Popović S, Valente-Feliciano A M, Phillips L and Vušković L 2014 *Physical Review Special Topics - Accelerators and Beams* **17** 122001 ISSN 1098-4402 URL https://link.aps.org/doi/10.1103/PhysRevSTAB.17.122001

[13] Rauf S and Kushner M J 1998 *Journal of Applied Physics* **83** 5087–5094 ISSN 0021-8979, 1089-7550 URL https://pubs.aip.org/jap/article/83/10/5087/487752/The-effect-of-radio-frequency-plasma-processing

[14] Cao D, Yu S, Chen Z, Wang Y, Wang H, Chen Z, Jiang W and Zhang Y 2024 *Journal of Vacuum Science & Technology A* **42** 013001 ISSN 0734-2101, 1520-8559 URL https://pubs.aip.org/jva/article/42/1/013001/2930732/Optimizing-impedance-matching-parameters-for

[15] Chabert P, Abada H, Booth J P and Lieberman M A 2003 *Journal of Applied Physics* **94** 76–84 ISSN 0021-8979, 1089-7550 URL https://pubs.aip.org/jap/article/94/1/76/483119/Radical-dynamics-in-unstable-CF4-inductive

[16] Katsch H M, Goehlich A, Kawetzki T, Quandt E and Döbele H F **75** 2023–2025 ISSN 0003-6951, 1077-3118 URL https://pubs.aip.org/apl/article/75/14/2023/109215/Attachment-induced-ionization-instability-of-a

[17] Despiau-Pujo E and Chabert P 2009 *Plasma Sources Science and Technology* **18** 045028 ISSN 0963-0252, 1361-6595 URL https://iopscience.iop.org/article/10.1088/0963-0252/18/4/045028

[18] Kawamura E, Lieberman M A, Lichtenberg A J and Graves D B **21** 045014 ISSN 0963-0252, 1361-6595 URL https://iopscience.iop.org/article/10.1088/0963-0252/21/4/045014

[19] Chabert P, Lichtenberg A J, Lieberman M A and Marakhtanov A M 2001 *Plasma Sources Science and Technology* **10** 478–489 ISSN 0963-0252, 1361-6595 URL https://iopscience.iop.org/article/10.1088/0963-0252/10/3/313

[20] Mussenbrock T, Brinkmann R P, Lieberman M A, Lichtenberg A J and Kawamura E 2008 *Phys. Rev. Lett.* **101**(8) 085004 URL https://link.aps.org/doi/10.1103/PhysRevLett.101.085004

[21] Schulze J, Kampschulte T, Luggenhölscher D and Czarnetzki U 2007 *Journal of Physics: Conference Series* **86** 012010 URL https://dx.doi.org/10.1088/1742-6596/86/1/012010

[22] Schüngel E, Brandt S, Donkó Z, Korolov I, Derzsi A and Schulze J 2015 *Plasma Sources Science and Technology* **24** 044009 URL https://dx.doi.org/10.1088/0963-0252/24/4/044009

[23] Kim S, Zhou Z, Lieberman M A and Lichtenberg A J 2006 *Journal of Applied Physics* **100** 103302 ISSN 0021-8979, 1089-7550 URL https://pubs.aip.org/jap/article/100/10/103302/394915/Relaxation-oscillations-in-a-capacitive-discharge

[24] Küllig C, Wegner T and Meichsner J 2015 *Physics of Plasmas* **22** 043515 ISSN 1070-664X, 1089-7674 URL https://pubs.aip.org/pop/article/22/4/043515/594958/Instabilities-in-a-capacitively-coupled-oxygen

[25] Dong W, Zhang Y F, Dai Z L, Schulze J, Song Y H and Wang Y N 2022 *Plasma Sources Science and Technology* **31** 025006 ISSN 0963-0252, 1361-6595 URL https://iopscience.iop.org/article/10.1088/1361-6595/ac47e4

[26] Brackbill J and Forslund D 1982 *Journal of Computational Physics* **46** 271–308 ISSN 0021-9991 URL https://www.sciencedirect.com/science/article/pii/002199918290016X

[27] Cohen B I, Langdon A and Friedman A 1982 *Journal of Computational Physics* **46** 15–38 ISSN 0021-9991 URL https://www.sciencedirect.com/science/article/pii/002199918290002X

[28] yu Wang H, Jiang W and nian Wang Y 2010 *Plasma Sources Science and Technology* **19** 045023 URL https://dx.doi.org/10.1088/0963-0252/19/4/045023

[29] Wu H, Zhou Y, Gao J, Peng Y, Wang Z and Jiang W 2021 *Plasma Sources Science and Technology* **30** 065029 URL https://dx.doi.org/10.1088/1361-6595/abff74

[30] Turner M M, Derzsi A, Donkó Z, Eremin D, Kelly S J, Lafleur T and Mussenbrock T

2013 *Physics of Plasmas* **20** 013507 ISSN 1070-664X (*Preprint* https://pubs.aip.org/aip/pop/article-pdf/doi/10.1063/1.4775084/13430854/013507_1_online.pdf) URL https://doi.org/10.1063/1.4775084

[31] Vass M, Palla P and Hartmann P **31** 064001 ISSN 0963-0252, 1361-6595 URL https://iopscience.iop.org/article/10.1088/1361-6595/ac6e85

[32] Wen D Q, Krek J, Gudmundsson J T, Kawamura E, Lieberman M A, Zhang P and Verboncoeur J P 2023 *Plasma Sources Science and Technology* **32** 064001 URL https://dx.doi.org/10.1088/1361-6595/acd6b4

[33] Roberto M, Smith H and Verboncoeur J 2003 *IEEE Transactions on Plasma Science* **31** 1292–1298 URL https://dx.doi.org/10.1109/TPS.2003.820682

[34] Lauro-Taroni L, Turner M M and Braithwaite N S 2004 *Journal of Physics D: Applied Physics* **37** 2216 URL https://dx.doi.org/10.1088/0022-3727/37/16/002

[35] Wang L, Hartmann P, Donkó Z, Song Y H and Schulze J 2021 *Journal of Vacuum Science & Technology A* **39** 063004 ISSN 0734-2101 (*Preprint* https://pubs.aip.org/avs/jva/article-pdf/doi/10.1116/6.0001327/15934134/063004_1_online.pdf) URL https://doi.org/10.1116/6.0001327

[36] Zheng B, Fu Y, qi Wen D, Wang K, Schuelke T and Fan Q H 2020 *Journal of Physics D: Applied Physics* **53** 435201 URL https://dx.doi.org/10.1088/1361-6463/ab9f68

[37] Yamabe C, Buckman S J and Phelps A V **27** 1345–1352 ISSN 0556-2791 URL https://link.aps.org/doi/10.1103/PhysRevA.27.1345

[38] Phelps A V **76** 747–753 ISSN 0021-8979, 1089-7550 URL https://pubs.aip.org/jap/article/76/2/747/496530/The-application-of-scattering-cross-sections-to

[39] See https://us.lxcat.net/contributors/#d19

[40] See https://github.com/PhysicsPlasma/iPM1D2019

[41] Yu S, Chen Z, Wu H, Guo L, Wang Z, Jiang W and Zhang Y 2022 *Journal of Applied Physics* **132** 083302 ISSN 0021-8979, 1089-7550 URL https://aip.scitation.org/doi/10.1063/5.0096910

[42] Yu S, Wu H, Xu J, Wang Y, Gao J, Wang Z, Jiang W and Zhang Y 2023 *Computer Physics Communications* **282** 108468 URL https://doi.org/10.1016/j.cpc.2022.108468

[43] Lafleur T, Chabert P and Bourdon A **130** 053305 ISSN 0021-8979, 1089-7550 URL https://pubs.aip.org/jap/article/130/5/053305/1079083/The-origin-of-the-breathing-mode-in-Hall-thrusters

[44] Hara K **28** 044001 ISSN 1361-6595 URL https://iopscience.iop.org/article/10.1088/1361-6595/ab0f70

[45] Choueiri E Y **8** 1411–1426 ISSN 1070-664X, 1089-7674 URL https://pubs.aip.org/pop/article/8/4/1411/264786/Plasma-oscillations-in-Hall-thrusters

[46] Boeuf J P **121** 011101 ISSN 0021-8979, 1089-7550 URL https://pubs.aip.org/jap/article/121/1/011101/145334/Tutorial-Physics-and-modeling-of-Hall-thrusters

[47] Ginoux J M and Letellier C **22** 023120 ISSN 1054-1500, 1089-7682 URL https://pubs.aip.org/cha/article/22/2/023120/322444/Van-der-Pol-and-the-history-of-relaxation

[48] Lawandy N **18** 1992–1994 ISSN 0018-9197 URL http://ieeexplore.ieee.org/document/1071492/

[49] Kononenko L I **1** 45–49 ISSN 1990-4789, 1990-4797 URL http://link.springer.com/10.1134/S199047890701005X